Statistical properties of time-dependent wave functions for classically chaotic bound and scattering systems

Boon Leong Lan, Anatolii Shushin, and David M. Wardlaw
Department of Chemistry, Queen's University, Kingston, Ontario, Canada K7L 3N6
(Received 12 February 1992)

Statistical properties of time-dependent wave functions for classically chaotic bound and scattering systems with two degrees of freedom are studied numerically and analytically. For comparison, two-dimensional systems that are classically nonchaotic are also studied numerically. Our numerical results show that the wave functions for chaotic systems become spatially irregular after some characteristic time, whereas no evident irregularities are observed in the nonchaotic systems. Spatial fluctuations of irregular wave functions are shown to be reproduced quite accurately by the random plane-wave superposition approximation. This approximation predicts that the real and imaginary parts of an irregular wave function are uncorrelated Gaussian stochastic functions with the same spatial pair correlation function, which is expressed through a Bessel function. To assess this prediction, distribution functions and spatial pair distribution functions for each of the real and imaginary parts, which must be Gaussian for Gaussian stochastic functions, are computed numerically and found to be close to Gaussian. Analysis of the widths of the numerical pair distribution functions enables us to obtain a pair correlation function that is, in accordance with prediction, well approximated by the Bessel function.

PACS number(s): 05.45.+b, 03.65.Bz, 02.50.+s, 02.70.+d

I. INTRODUCTION

The quantum study of bound and unbound (scattering) systems that exhibit chaos classically is an area of research often referred to as quantum chaos. For bound systems (see Eckhardt [1] for a review and a comprehensive list of references), such studies are either time independent (statistical properties of energy eigenvalues and eigenfunctions) or time dependent (time evolution of wave packet and observables). For scattering systems, the S matrix [2–5] has been the focus of investigations so far. For reviews and additional references on classical and quantum chaotic scattering, see Eckhardt [6], Smilansky [7], Blumël [8], and Weidenmüller [9]. Numerical and experimental evidence accumulated so far indicate that the statistics of energy levels and the statistical properties of the S matrix exhibit universality. In particular, they follow the predictions of random matrix theory [1,4,7,8].

Statistical properties of eigenfunctions also exhibit universality. Numerical studies of real-valued eigenfunctions ϕ for two-dimensional classically chaotic bound systems [10–12] have shown that the distribution function (denoted as DF throughout this paper) $P(\phi)$ provides a quantitative diagnostic for distinguishing spatially regular and irregular states. Irregular eigenfunctions have $P(\phi)$, which are well approximated by Gaussians, but $P(\phi)$ for regular eigenfunctions are non-Gaussians. Furthermore, the spatial pair correlation function (denoted as PCF) $\langle \phi(\mathbf{r}_1)\phi(\mathbf{r}_2)\rangle$ of an irregular eigenfunction is given in terms a zeroth-order Bessel function of the first kind whose argument depends only on the energy and $|\mathbf{r}_1-\mathbf{r}_2|$ [11,13]. A similar property of the PCF was also obtained for time-dependent wave function for the stadium billiard [13]. These results were predicted by Berry [14] with the assumption that an irregular eigenfunction is well approximated by a superposition of random plane waves. We shall refer to this approximation as the PWSA (plane-wave superposition approximation).

In this paper, we apply the PWSA to complex-valued time-dependent wave functions ψ for classically chaotic bound and scattering systems with two degrees of freedom. Through our numerical studies, we found that the wave function eventually becomes spatially irregular. Using the PWSA, we show that the real part and the imaginary part of an irregular wave function are uncorrelated Gaussian [15] stochastic functions; i.e., the DFs of the real part $P(\mathrm{Re}(\psi))$ and the imaginary part $P(\mathrm{Im}(\psi))$ are Gaussians with the same width and $\langle \mathrm{Re}(\psi)\rangle = \langle \mathrm{Im}(\psi)\rangle = 0$, the spatial pair distribution functions (denoted as PDF) $P(\mathrm{Re}(\psi_1),\mathrm{Re}(\psi_2),|\mathbf{r}_1-\mathbf{r}_2|)$ and $P(\mathrm{Im}(\psi_1),\mathrm{Im}(\psi_2),|\mathbf{r}_1-\mathbf{r}_2|)$, are Gaussians, and so are all corresponding higher-order distribution functions. Furthermore, the PCF of the real part (and the imaginary part) is given in terms of a zeroth-order Bessel function of the first kind. Numerical evidence in support of our analytic results is provided. In particular, the numerical DF, PDF, and PCF agree well with the predictions of the PWSA.

To propagate the wave packet, the time-dependent Schrödinger equation is integrated numerically. In Sec. II, we will present the models and discuss the method of integration and the choice of initial wave packets. The PWSA will be discussed in Sec. III. Results are presented and discussed in Sec. IV.

II. MODELS, NUMERICAL METHOD, AND INITIAL WAVE PACKET

The potentials we have chosen for wave-packet scattering are shown in Fig. 1. Regions I, II, and III are regions

 ©1992 The American Physical Society

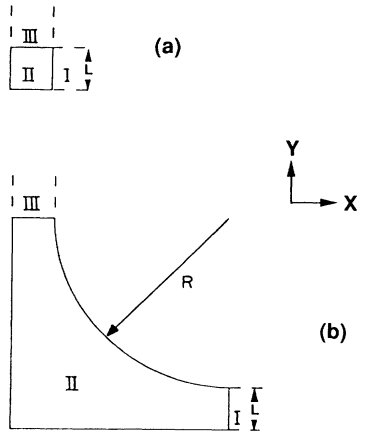

FIG. 1. L-shaped potential (a) and elbow-shaped potential (b). The box billiard and the $S4$ billiard are defined by the interaction regions II in (a) and (b), respectively. $R=0.2$ and $L=0.05$.

of zero potential energy; outside the boundaries, the potential energy is infinite. Regions II will be referred to as the interaction regions. The L-shaped potential [Fig. 1(a)] was first introduced by Hulburt and Hirschfelder [16] in 1943 as an idealized model potential for collinear three-body rearrangement scattering $A+BC\rightarrow AB+C$. Classical scattering by this potential does not exhibit chaos. A potential that exhibits chaotic scattering classically (the final vibrational action versus initial vibrational phase displays fluctuations on all scales of the initial conditions and the distribution of dwell time in the interaction region is exponential [17]) is shown in Fig. 1(b). Variants of this elbow-shaped potential have recently been studied [5]; e.g., for the case in which the potential in region III is infinite (the classical dwell-time distribution is also exponential), the S matrix was studied in a microwave-scattering experiment and also numerically. For bound systems, billiards defined by the interaction regions II in Figs. 1(a) and 1(b) are chosen. Classically, the box billiard in Fig. 1(a) is an integrable system while the $S4$ billiard (we call it $S4$ since it is one-fourth of Sinai's billiard) in Fig. 1(b) is chaotic.

Within the potential-free region, the time-dependent Schrödinger equation ($\hbar=1, m=1$) has the form

$$i\frac{\partial\psi(x,y)}{\partial t}=H\psi(x,y)\ , \tag{1}$$

where

$$H=-\frac{1}{2}\left[\frac{\partial^2}{\partial x^2}+\frac{\partial^2}{\partial y^2}\right]\ .$$

Formally, Eq. (1) has the solution

$$\psi(x,y,t)=\exp(-iHt)\psi(x,y,0)\ . \tag{2}$$

One method [18] of obtaining an explicit integration scheme is to expand the time evolution operator $\exp(-iH\delta)$ in a Taylor series

$$\exp(-iH\delta)\approx 1-iH\delta-\tfrac{1}{2}(H\delta)^2\ , \tag{3}$$

which is accurate to second order in time δ, and replace the second derivatives in $H\psi$ by second-order finite difference formulas

$$\frac{\partial^2\psi^n j,k}{\partial x^2}=\Delta^{-2}(\psi^n_{j+1,k}-2\psi^n_{j,k}+\psi^n_{j-1,k}) \tag{4}$$

and

$$\frac{\partial^2\psi^n j,k}{\partial y^2}=\Delta^{-2}(\psi^n_{j,k+1}-2\psi^n_{j,k}+\psi^n_{j,k-1})\ . \tag{5}$$

$\psi^n_{j,k}$ denotes the wave-function value at time $n\delta$ ($n=0,1,2,\ldots$) and grid point ($x_j=j\Delta$ ($j=0,1,2,\ldots$), $y_k=k\Delta$ ($k=0,1,2,\ldots$)), where Δ is the grid spacing. Because this scheme is unconditionally unstable [18], it cannot be used for more than a few time steps.

A conditionally stable, explicit integration scheme given by Harmuth [19] for one dimension, and later extended to two dimensions by Askar and Cakmak [20], can be obtained [21] by substituting the following second-order finite difference formula for the time derivative

$$\frac{\partial\psi^n j,k}{\partial t}=\frac{1}{2\delta}(\psi^{n+1}_{j,k}-\psi^{n-1}_{j,k}) \tag{6}$$

into Eq. (1), yielding

$$\psi^{n+1}_{j,k}=\psi^{n-1}_{j,k}-2i\delta H\psi^n_{j,k} \tag{7}$$

and replacing the second derivatives in $H\psi$ in the expression above by Eqs. (4) and (5). The resulting scheme is stable if [21,22]

$$\frac{\delta}{\Delta^2}\leq\frac{1}{4}\ . \tag{8}$$

To use this scheme, the values of ψ at $t=\delta$ are also needed in addition to their initial values. In our numerical studies, they were obtained using the unstable scheme [Eq. (3)].

For wave-packet scattering, the initial wave packet was chosen to represent a free atom A approaching a molecule BC in its ground vibrational state

$$\psi(x,y,0)=\psi_t(x)\psi_v(y)\ , \tag{9}$$

where the translational part is a normalized Gaussian

$$\psi_t(x)=\left[2\pi\sigma^2\right]^{-(1/4)}\exp\left[\frac{-(x-x_0)^2}{4\sigma^2}\right]\exp(ik_x x) \tag{10}$$

and the vibrational part is the ground-state eigenfunction for a one-dimensional box of width L

$$\psi_v(y)=\left[\frac{2}{L}\right]^{1/2}\sin\left[\frac{\pi y}{L}\right]\ . \tag{11}$$

The values of x_0 and σ were chosen such that the wave packet was localized in region I, and k_x was chosen such that the wave packet was moving towards region II initially.

For the bound billiard systems, the initial wave packet was chosen to be a normalized two-dimensional Gaussian

$$\psi(x,y,0)=(2\pi\sigma^2)^{-(1/2)}\exp\left[\frac{-(x-x_0)^2-(y-y_0)^2}{4\sigma^2}\right]\times\exp(ik_x x+ik_y y)\ . \quad (12)$$

The values of x_0, y_0, and σ were chosen so that ψ was essentially zero on the boundary of the billiard.

With the above choices of initial wave packets, the grid spacing Δ was chosen to be much less than the smallest de Broglie wavelength (the wavelength is $2\pi/p$, where p is the momentum associated with the initial wave packets), and the time step δ was chosen such that the stability condition (8) was satisfied.

III. THEORETICAL TREATMENT

Here we investigate some general and universal properties of spatially irregular wave packets within the PWSA. The assumption is that the irregularity of wave functions results from the fact that at each point of space the wave function is a superposition of a very large number of plane waves with similar amplitudes and uncorrelated relative phases [14]. As we have mentioned in the Introduction, the PWSA has been applied to real-valued eigenfunctions for bound systems. Time-dependent was packets are, however, complex valued. Thus the problem is to describe the properties of both real and imaginary parts of the wave packets. We shall show in this section that the PWSA can be successfully applied to the analysis of wave packets as well. Before we do so, we shall first obtain some properties of PCF by considering general properties of wave-packet evolution in time.

A. General considerations of PCF

First, let us consider a bound system. For simplicity of discussion we shall take a two-dimensional billiard. The time-dependent wave function can be represented by

$$\psi(\mathbf{r},t)=\sum_n a_n\psi_n(\mathbf{r})e^{-i\varepsilon_n t}\ , \quad (13)$$

where $\psi_n(\mathbf{r})$ are (real) eigenfunctions of the system corresponding to eigenfunctions ε_n and the amplitudes

$$a_n=\langle\psi_0|\psi_n\rangle=|a_n|\exp(-i\theta_n) \quad (14)$$

are determined by the initial wave function $\psi_0(\mathbf{r})$ [see Eq. (12)].

In general, the PCF $C[\psi,\psi](l)$ at time t is defined by

$$C[\psi,\psi](l)=S^{-1}\mathrm{Re}\left[\int_S d\mathbf{r}\,\psi^*(\mathbf{r},t)\psi(\mathbf{r}+l,t)\right]\ . \quad (15)$$

The size of the integration area S should be taken much larger than the characteristic length of spatial correlations of $\psi(\mathbf{r},t)$. In particular, for a two-dimensional billiard, it is convenient to take S to be equal to the total area of the billiard. In principle, if the wave-function spatial fluctuations are homogeneous, then $C[\psi,\psi]$ is independent of the size of S and its location in the whole area of homogeneous irregularity.

Now let us introduce two real functions

$$\chi(\mathbf{r},t)=\mathrm{Re}\psi(\mathbf{r},t),\quad \eta(\mathbf{r},t)=\mathrm{Im}\psi(\mathbf{r},t)\ , \quad (16)$$

and discuss the spatial stochastic behavior of $\psi(\mathbf{r},t)$ in terms of the corresponding stochastic properties of the functions $\chi(\mathbf{r},t)$ and $\eta(\mathbf{r},t)$. In particular, we shall consider PCFs of $\chi(\mathbf{r},t)$ and $\eta(\mathbf{r},t)$. For $C[\chi,\chi]$, we have

$$C[\chi,\chi]=\sum_{n,n'}|a_n a_{n'}|C[\psi_n,\psi_{n'}]\cos(\varepsilon_n t+\theta_n)\times\cos(\varepsilon_{n'}t+\theta_{n'})\ . \quad (17)$$

$C[\chi,\chi]$ has two parts: a time-dependent one and a time-independent one (arising from the sum over $n=n'$). Numerical calculation shows (see next section) that for a smooth wave packet, the time-dependent part decreases rapidly with the increase of time. We believe this is due to the interference of strongly oscillating terms, so that at long times we observe only the steady-state spatial fluctuations of $\chi(\mathbf{r},t)$ and thus

$$C[\chi,\chi]=\tfrac{1}{2}\sum_n|a_n|^2C[\psi_n,\psi_n]\ . \quad (18)$$

Formulas similar to (17) can also be written for $C[\eta,\eta]$ and $C[\chi,\eta]$. The same arguments lead us to the conclusion that at large times

$$C[\eta,\eta]=C[\chi,\chi] \quad (19)$$

and

$$C[\chi,\eta]=C[\eta,\chi]=0\ . \quad (20)$$

Due to the smooth dependence of $C[\psi_n,\psi_n]$ on ε_n, we can write, in the case of small dispersion of energies in the wave packet,

$$C[\chi,\chi]=C[\eta,\eta]\simeq C[\psi_E,\psi_E]\ , \quad (21)$$

where ψ_E is the eigenfunction corresponding to the eigenvalue ε_n, which is closest to the most probable energy E of the wave packet. Numerical calculations confirm the validity of relations (19) and (20) (see next section). Formula (21) reduces the problem of calculation of the wave-packet spatial PCF to calculation of the eigenfunction PCF. This means that any approximation (e.g., PSWA) that accurately describes the PCF of the eigenfunction also describes the PCF of the wave packet correctly. A similar method of expansion in eigenfunctions was applied in [13] to a PCF of the wave function itself (not just real and imaginary parts separately, as in our case).

Additional arguments in favor of relation (20) can be obtained by considering the flux density. Relation (20) implies the absence of average fluxes in the system. The flux density is

$$\mathbf{J}=(1/2i)(\psi^*\nabla\psi-\psi\nabla\psi^*)=(\chi\nabla\eta-\eta\nabla\chi)\ . \quad (22)$$

It is easily seen that if $C[\eta,\chi]=C[\chi,\eta]=0$, then $C[\chi,\nabla\eta]=C[\eta,\nabla\chi]=0$. Thus

$$\langle\mathbf{J}\rangle=C[\chi,\nabla\eta]-C[\eta,\nabla\chi]=0\ . \quad (23)$$

Intuitively, this result is quite reasonable if we take into account that irregular wave-function spatial behavior is associated with classically chaotic systems in which a classical trajectory passes through any small area many

times in arbitrary directions, thus giving only a small contribution to the average flux through this area.

A similar qualitative analysis can be done for the scattering problem as well. In this case, ψ_n can be associated with some basis of discrete eigenfunctions, complete in the interaction area supporting the irregular behavior. However, due to the finiteness of the dwell time in the interaction region, we cannot use the above arguments concerning the asymptotic time independence of the fluctuations of $\chi(\mathbf{r},t)$ nd $\eta(\mathbf{r},t)$. But the statement about the stochastic independence of their spatial fluctuations is supported by qualitative arguments concerning the average flux [see Eq. (23)] and numerical evidence. It is clear that in a scattering system, the average flux is nonzero so that fluctuations of $\chi(\mathbf{r},t)$ and $\eta(\mathbf{r},t)$ are in principle correlated, but for classically chaotic systems this correlation is rather small, giving a nonzero average flux much smaller than fluctuations of the flux itself.

The idea of this subsection is to demonstrate that after some time of evolution, there is some decoupling, as expressed by Eq. (20), of the spatial fluctuations of irregular wave functions. This will be demonstrated again below, using the PSWA.

B. Plane-wave superposition approximation (PWSA)

Here we obtain spatial correlation functions of time-dependent wave functions using the PWSA [14]. It is clear, however, that the PWSA becomes valid only after some initial period of "relaxation" toward irregularity. In this subsection, we consider the properties of wave functions at given times; thus for brevity in what follows, we shall omit the time argument of all functions considered.

According to the PWSA, the wave function $\psi(\mathbf{r})$ can be represented by

$$\psi(\mathbf{r})=\sum_{j=1}^{N}(A_j/\sqrt{N})\exp[ik(\mathbf{n}_j\cdot\mathbf{r})+i\theta_j]\ , \tag{24}$$

where $k=|\mathbf{k}_j|=\sqrt{E}\ /2$ is the absolute value of the wave vector, $\mathbf{n}_j=\mathbf{k}_j/k$ are unit vectors in the direction of $\mathbf{k}_j$, A_j are real amplitudes of the plane waves (assumed to be of the same order of magnitude), and θ_j are relative phases of the waves distributed randomly over the interval $(0,2\pi)$. The parameters of the plane waves are time dependent (except for k), but here we are not going to analyze time correlations and thus ignore their time dependence. Both A_j and θ_j are taken to be independent of $\mathbf{r}$. In reality they may depend on $\mathbf{r}$ but the characteristic scale of this dependence is on the order of the size $\sqrt{S}$ of the billiard, while the scale of effects considered below is the wavelength $\lambda=k^{-1}\ll\sqrt{S}$. Thus we can neglect A_j and θ_j dependences on $\mathbf{r}$. Note that unlike eigenfunctions of bound systems, any time-dependent wave function is complex, and no *a priori* constraints can be imposed on the parameters of representation (24).

Now let us consider the stochastic properties of $\chi(\mathbf{r})=\mathrm{Re}\psi(\mathbf{r})$ and $\eta(\mathbf{r})=\mathrm{Im}\psi(\mathbf{r})$ predicted by representation (24). It is easily seen that

$$C[\chi,\eta]=\langle\chi(\mathbf{r})\eta(\mathbf{r}')\rangle_{\mathbf{n}_j,\theta_j}=0\ , \tag{25}$$

in agreement with Eq. (20). The angular brackets in Eq. (25) denote an average over the directions $\mathbf{n}_j$ and over the phases θ_j. Hereafter, for brevity, we shall omit subscripts $\mathbf{n}_j$ and θ_j from our notation for averaging. Thus the PWSA predicts statistical independence of spatial $\chi(\mathbf{r})$ and $\eta(\mathbf{r})$ fluctuations so that we can describe them separately.

Some additional comments on the PWSA and in particular on the expression (25) are needed at this point. In the previous section [Eq. (15)] we defined PCF's as averages (integrals) over the area in which the wave function is irregular. Here they are replaced by averages over $\mathbf{n}_j$ and θ_j. These two types of seemingly different averages are, however, closely connected. Integration over the area at a given $|\mathbf{r}-\mathbf{r}'|=l$ would result in $\delta(\mathbf{k}_j-\mathbf{k}_{j'})\sim\delta_{jj'}$ terms, but the same terms also arise due to integration over independent stochastic variables θ_j. Moreover, there is another more fundamental relation between these two kinds of averages. The PWSA ascribes continuous distributions to $\mathbf{n}_j$ and θ_j at each point in space. That is not actually the case because at each point, $\psi(\mathbf{r})$ results from the interference of only a finite number (which may not be large) of plane waves (ensemble of waves). The continuous distributions, however, arise when we consider the whole area of wave-function irregularity because the irregularity implies that the ensemble of plane waves is different at different parts of the area. An average over the area is equivalent to an average over the ensembles of plane waves corresponding to different parts of the area, and hence over continuous distributions of $\mathbf{n}_j$ and θ_j. The correspondence of these two kinds of averages also implies the dependence of any PCF, say PCF (25), only on $l=|\mathbf{r}-\mathbf{r}'|$ and not on $\mathbf{r}$ and $\mathbf{r}'$ themselves. This will be demonstrated below [see Eq. (28)].

According to the central limit theorem, both $\chi(\mathbf{r})$ and $\eta(\mathbf{r})$ are Gaussian stochastic functions (Gaussian stochastic processes in $\mathbf{r}$) [15]. To prove this statement, say for $\chi(\mathbf{r})$, let us consider the generating functional

$$F[f]=\left\langle\exp\left[i\int d\mathbf{r}\,f(\mathbf{r})\chi(\mathbf{r})\right]\right\rangle\ , \tag{26}$$

where $f(\mathbf{r})$ is some smooth trial function localized in S. Substituting expression (24) for $\chi(\mathbf{r})=\mathrm{Re}\psi(\mathbf{r})$ into Eq. (26) we get in the limit $N\gg1$

$$\begin{aligned}F[f]&\simeq\prod_j\left\{\left\langle1-\frac{1}{2}\frac{A_j^2}{N}\int d\mathbf{r}\int d\mathbf{r}'f(\mathbf{r})f(\mathbf{r}')\cos[k(\mathbf{n}_j\mathbf{r})+\theta_j]\cos[k(\mathbf{n}_j\mathbf{r}')+\theta_j]\right\rangle\right\}\\&\simeq\exp\left\{-\tfrac{1}{2}\int d\mathbf{r}\int d\mathbf{r}'C[\chi,\chi](\mathbf{r}-\mathbf{r}')f(\mathbf{r})f(\mathbf{r}')\right\}\ ,\end{aligned} \tag{27}$$

TABLE I. Parameter values for the initial wave packets and finite difference scheme, together with "earlier" and "later" time values for each of the four models studied.

Parameter	Box billiard	L-shaped	$S4$ billiard	Elbow-shaped
σ^2	6.25×10^{-6}	2.5×10^{-5}	6.25×10^{-6}	2.5×10^{-5}
x_0	0.025	0.1	0.076	0.3
y_0	0.025		0.076	
k_x	800	-400	800	-400
k_y	800		800	
Δ	5×10^{-4}	5×10^{-4}	5×10^{-4}	10^{-3}
δ	4×10^{-8}	4×10^{-8}	4×10^{-8}	10^{-7}
Earlier time	4.6×10^{-5}	1.5×10^{-4}	2.5×10^{-4}	1.5×10^{-3}
Later time	1.6×10^{-4}	3×10^{-4}	6×10^{-4}	2.5×10^{-3}

where

$$C[\chi,\chi](\mathbf{r}-\mathbf{r}')=\langle\chi(\mathbf{r})\chi(\mathbf{r}')\rangle=\langle\chi^2\rangle J_0(k|\mathbf{r}-\mathbf{r}'|)\ , \tag{28}$$

J_0 is a zeroth-order Bessel function of the first kind and

$$C[\chi,\chi](0)=\langle\chi^2\rangle=\left[\sum_j A_j^2/N\right]/2=\overline{A^2}/2\ . \tag{29}$$

For billiard systems, if we take S to the whole area, we get [11]

$$C[\chi,\chi](0)=(1/S)\int d\mathbf{r}\,\chi^2(\mathbf{r})=1/2S\ .$$

In deriving expressions (27)–(29), we have used the evident relations

$$\langle\cos[k(\mathbf{n}_j\cdot\mathbf{r})+\theta_j]\rangle=0 \tag{30}$$

and

$$\langle\cos[k(\mathbf{n}_j\cdot\mathbf{r})+\theta_j]\cos[k(\mathbf{n}_{j'},\mathbf{r}')+\theta_{j'}]\rangle=(\delta_{jj'}/2)\langle\cos\{k[\mathbf{n}_j\cdot(\mathbf{r}-\mathbf{r}')]\}\rangle\ . \tag{31}$$

Formula (27) is nothing else but the definition of a Gaussian process, i.e., $\chi(\mathbf{r})$ is actually a Gaussian function with PCF [15]

$$C[\chi,\chi](\mathbf{r}-\mathbf{r}')=-\frac{\delta}{\delta f(\mathbf{r})}\frac{\delta}{\delta f(\mathbf{r}')}F[f]|_{f(\mathbf{r})=f(\mathbf{r}')=0}\ . \tag{32}$$

Similar calculation shows that $\eta(\mathbf{r})$ is also a Gaussian function with

$$C[\eta,\eta]=C[\chi,\chi] \tag{33}$$

in agreement with relation (19).

Until now, only a Gaussian distribution of amplitudes (for some billiards) has been considered as a demonstration that an irregular eigenfunction is a Gaussian function [10,12]. However, the distribution of amplitudes is only a crude integral property of stochastic functions. A much more persuasive argument in favor of the Gaussian statistics of spatial fluctuations of $\chi(\mathbf{r})$ [and $\eta(\mathbf{r})$] is the Gaussian form of the PDF whose two widths are determined completely by the PCF. For any Gaussian function $\chi(\mathbf{r})$, the PDF is known to be [15]

$$P(\chi_1,\chi_2,|\mathbf{r}_1-\mathbf{r}_2|)=\langle\delta(\chi_1-\chi(\mathbf{r}_1))\delta(\chi_2-\chi(\mathbf{r}_2))\rangle=(1/2\pi\sqrt{\beta_+\beta_-})\times\exp[-(\chi_1-\chi_2)^2/4\beta_- -(\chi_1+\chi_2)^2/4\beta_+]\ , \tag{34}$$

where

$$\beta_\pm=\langle\chi^2\rangle[1\pm g(k|\mathbf{r}_1-\mathbf{r}_2|)] \tag{35}$$

and

$$g(kl)=C[\chi,\chi](l)/C[\chi,\chi](0)=J_0(kl)\ . \tag{36}$$

The same expression is valid for $P(\eta_1,\eta_2,|\mathbf{r}_1-\mathbf{r}_2|)$.

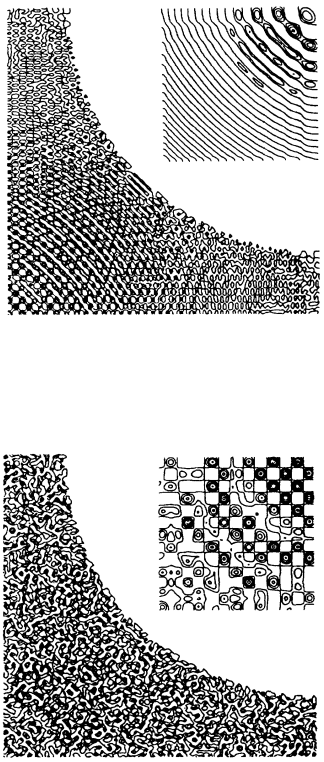

FIG. 2. Contours of positive $\mathrm{Re}(\psi)$ for the box and $S4$ billiard systems: (a) at earlier times; (b) at later times.

Formula (34) reveals the main property of Gaussian functions (Gaussian processes): any n-point distribution function of their amplitudes is Gaussian. In the next section, we shall verify the relations (25), (33), and (34)–(36) by comparison to numerical results.

IV. NUMERICAL RESULTS AND DISCUSSION

In order to demonstrate the difference between wave-function spatial behavior in classically chaotic and nonchaotic systems and to check the predictions of the previous section, wave-packet studies of two billiard systems and two scattering systems were done. The box billiard and L-shaped scattering systems [Fig. 1(a)] are classically nonchaotic, but the S4 billiard and elbow-shaped scattering systems [Fig. 1(b)] are chaotic. All the parameters used for wave-packet calculations are listed in Table I. All the distributions and averages introduced in the previous section were calculated by integration over the whole area for billiard systems and over the interaction region for scattering systems.

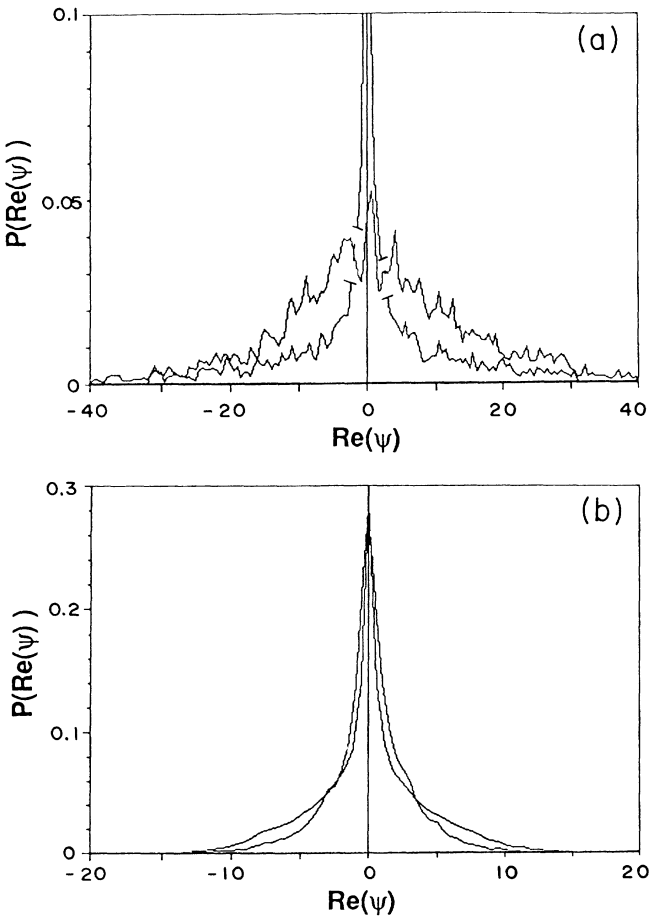

FIG. 3. Distribution functions $P(\mathrm{Re}(\psi))$ at earlier times for (a) box billiard (curve with higher peak, which extends beyond plot) and L-shaped scattering system; (b) $S4$ billiard (curve with narrower peak but wider base) and elbow-shaped scattering system. In (a), parts of the curve for the box billiard were removed so that the two curves are distinguishable.

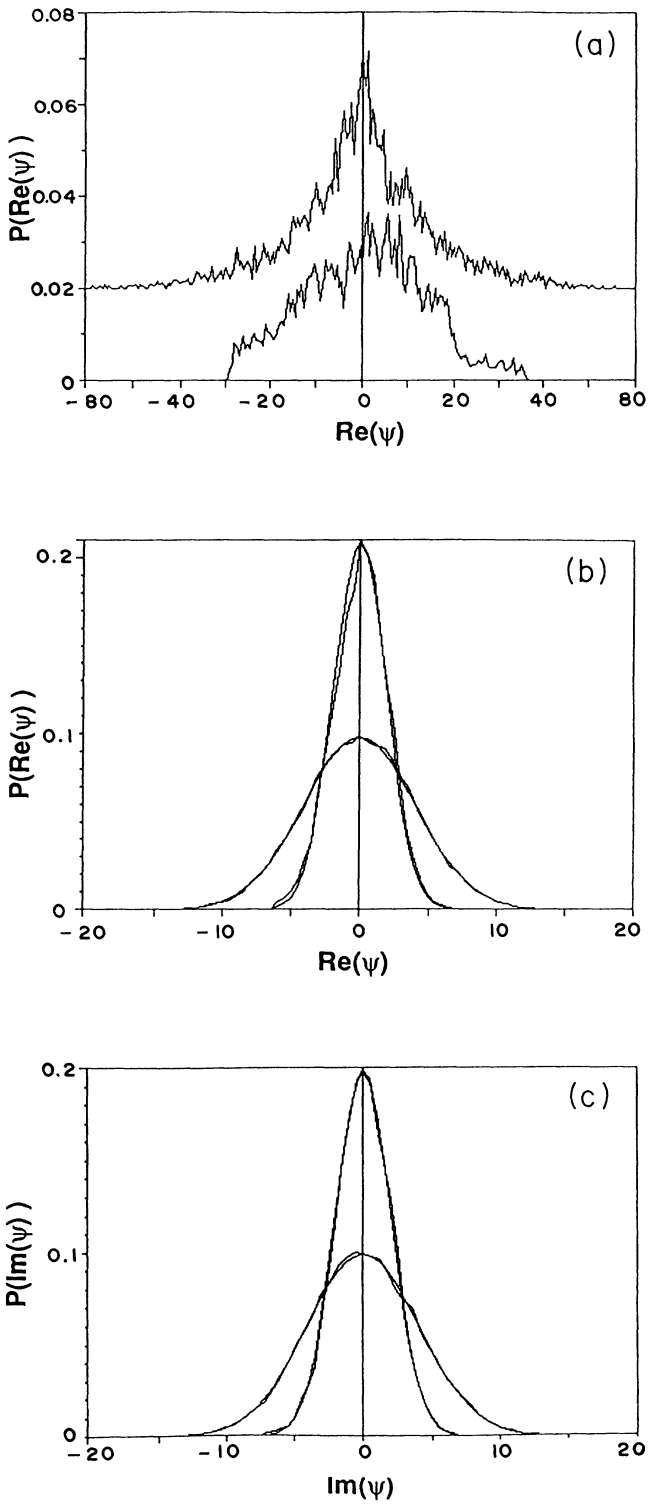

FIG. 4. Distribution functions $P(\mathrm{Re}(\psi))$ at later times for (a) the box billiard (upper curve) and the L-shaped scattering system (lower curve); (b) the $S4$ billiard (wider curve) and the elbow-shaped scattering system (narrower curve). $P(\mathrm{Re}(\psi))$ for the box billiard is vertically displaced by 0.02. The corresponding distribution functions $P(\mathrm{Im}(\psi))$ for the $S4$ billiard (wider curve) and the elbow-shaped scattering system (narrower curve) are shown in (c). In (b) and (c), normalized Gaussian fits are included for comparison with numerical distributions.

At earlier times (see Table I), the wave functions are regular in appearance in all four systems. For the billiard systems, this is illustrated in Fig. 2(a) by the contours of positive χ. The DF's $P(\chi)$ for all four systems are absolutely non-Gaussian (Fig. 3) and so are the functions $P(\eta)$ (not depicted). For the chaotic systems, the functions $P(\eta)$ are very similar to the corresponding functions $P(\chi)$.

At later times (see Table I), i.e., for times much longer than the characteristic dynamical time of the systems (time of flight between the walls), the wave functions for nonchaotic systems remain regular but the wave functions for chaotic systems become irregular [contours of positive χ are shown in Fig. 2(b) for the billiard systems]. The DF's $P(\chi)$ and $P(\eta)$ for the nonchaotic systems are still non-Gaussian [the DF's $P(\chi)$ are shown in Fig. 4(a)], but for the chaotic systems they approach Gaussians [Figs. 4(b) and 4(c)]. Note that in agreement with analytical considerations, the Gaussian DF's $P(\chi)$ and $P(\eta)$ for each of the chaotic systems are of the same width, and for the $S4$ billiard, the numerical variance agrees well with $1/2S$ as predicted. For the chaotic systems, the PDF's $P(\chi_1,\chi_2,l)$ are also Gaussian and the elliptical contours are oriented at 45° [Figs. 5(a) and 6(a)], in agreement with the prediction of Eq. (34). The corresponding PDF's $P(\eta_1,\eta_2,l)$ are also Gaussians with the same parameters. Finally, the contours of $P(\chi_1,\eta_2,l)$ shown in Fig. 7 are very close to concentric circles, indicating the absence of correlations between $\chi=\mathrm{Re}\psi$ and $\eta=\mathrm{Im}\psi$ for both chaotic systems.

Our numerical results for the $S4$ billiard and elbow-shaped scattering systems show that the DF's $P(\chi)$ and $P(\eta)$ are very well approximated by Gaussians [Figs. 4(b) and 4(c)], whereas the deviations from Gaussians for the PDF's (Figs. 5, 6, and 7) are more pronounced. This can be explained as follows. In each case, we used the same number of data points (χ or η grid values) to construct both the DF's and PDF's as normalized histograms. However, if N data points produce good statistics for the DF's then N^2 data points are needed for the PDF's. For the elbow-shaped scattering system, the number of data points in each histogram bin of the PDF was no more than 100. Thus, the statistical deviation is at least of the order of $(100)^{-1/2}=10\%$. Because the grid size for the $S4$ billiard is two times smaller than the grid size for the elbow-shaped scattering system, the deviation for the $S4$ billiard is expected to be two times smaller. Our numerical results support this expectation (compare Figs. 5 and 6). Unfortunately, any decrease in the grid size results in a large increase of computer memory needed to integrate

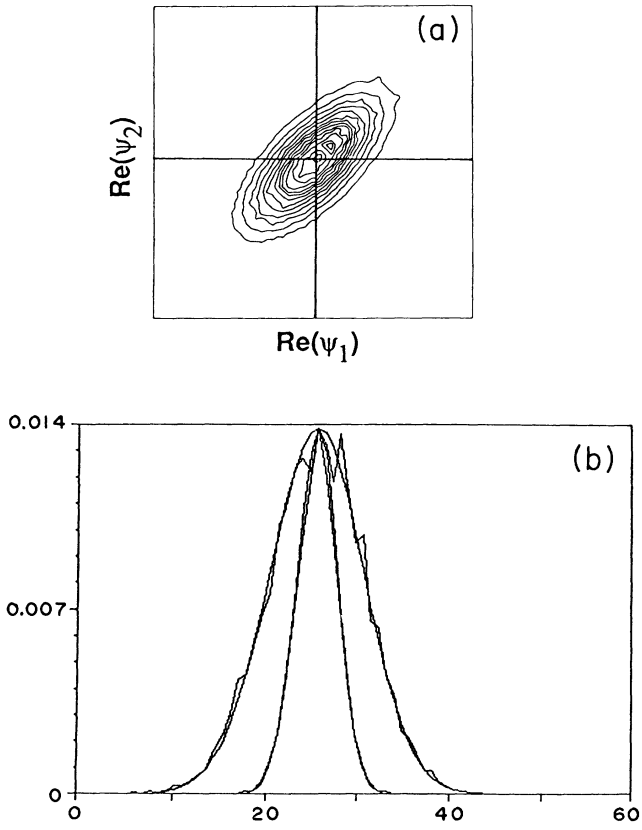

FIG. 5. Typical pair distribution function $P(\mathrm{Re}(\psi_1),\mathrm{Re}(\psi_2),l)$ for the $S4$ billiard ($l=10^{-3}$) at a later time: (a) contours; (b) cross sections along $\mathrm{Re}(\psi_2)=\mathrm{Re}(\psi_1)$ (wider curve) and along $\mathrm{Re}(\psi_2)=-\mathrm{Re}(\psi_1)$ (narrower curve). In (b), the corresponding cross sections of the Gaussian prediction (Eq. 34) are included for comparison; the horizontal axis is the distance along the diagonals in (a).

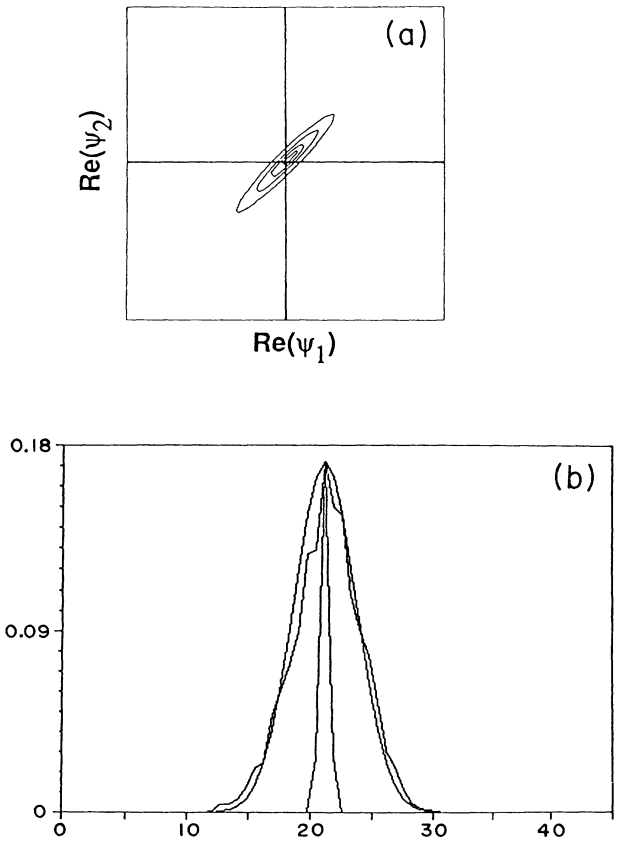

FIG. 6. Same as Fig. 5, but for the elbow-shaped scattering system ($l=10^{-3}$) at a later time.

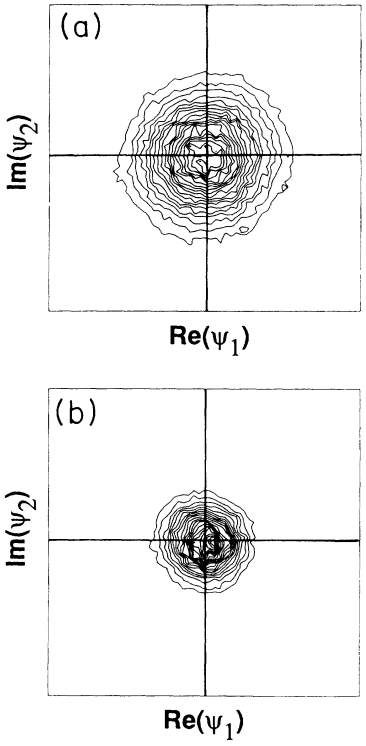

FIG. 7. Typical contours of the pair distribution functions $P(\mathrm{Re}(\psi_1),\mathrm{Im}(\psi_2),l)$ at later times for (a) the $S4$ billiard ($l=5\times10^{-4}$); (b) the elbow-shaped scattering system ($l=10^{-3}$).

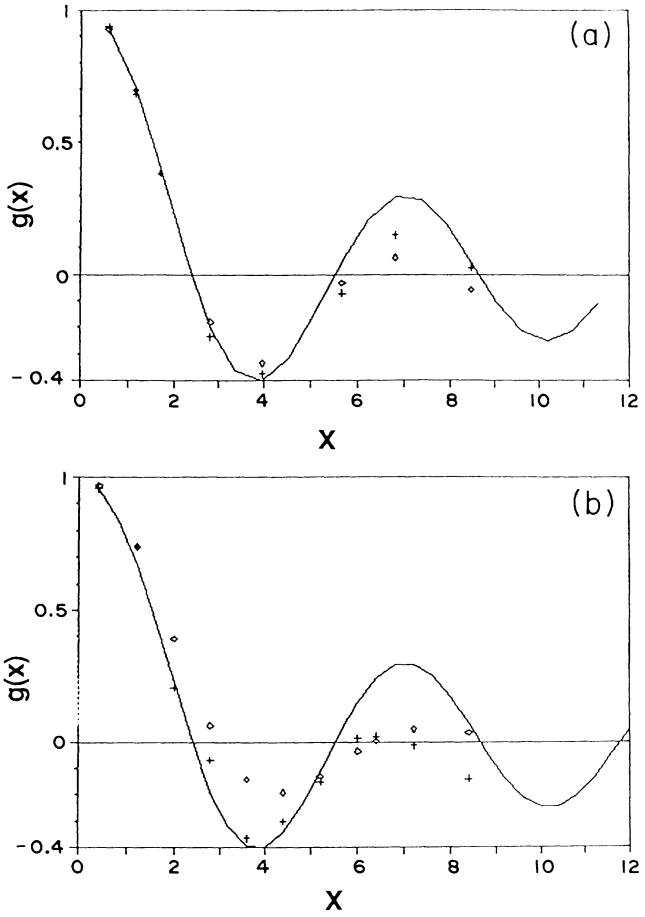

FIG. 8. (a) $g(x)$ extracted from the widths of the numerical pair distribution function $P(\mathrm{Re}(\psi_1),\mathrm{Re}(\psi_2),l)$ (crosses), and $g(x)$ computed directly from definition (diamonds) for the $S4$ billiard, where $x=kl$. The solid line is a zeroth-order Bessel function of the first kind $J_0(x)$. For (b), same as (a) but for the elbow-shaped scattering system.

the Schrödinger equation. We could not use a smaller grid size for the scattering system because the total area in which the equation has to be integrated is much larger than that of the corresponding billiard system and thus a lot more memory is required. This brief analysis shows that accurate calculation of the PDF's requires more numerical effort than the DF's.

The validity of the PWSA can be demonstrated more convincingly by extracting the quantity $g(kl)$ from the widths of the numerical PDF $P(\chi_1,\chi_2,l)$ for different l values and comparing it with the analytical expression (36). For both chaotic systems, the agreement between numerical and analytical $g(kl)$ is good, especially at small $x=kl$ (Fig. 8). The large deviations at large values of l [numerical $g(kl)$ amplitudes are smaller] are mainly due to the large spread of wave vectors k in the initial wave packet. In addition, we should also take into account that the plane-wave superposition is only an approximation, thus giving a somewhat incorrect prediction for $g(kl)$ at large l. Indeed, a similar discrepancy between numerical and analytical $g(kl)$ has been observed [11] for irregular eigenfunctions (without any spread in k by definition) of some chaotic bound systems and is believed to be due to the inaccuracy of the expression (36) at large distances. Finally, the aforementioned statistical error in constructing the numerical PDF's is another source of discrepancy between numerical and analytical $g(kl)$.

The quantity $g(kl)$ can be also obtained directly from the definition appearing in Eq. (36) by calculating the averages $\langle\chi(\mathbf{r})\chi(\mathbf{r}')\rangle$ and $\langle\chi^2(\mathbf{r})\rangle$. Although this method does not give us any information about higher-order correlation functions, it makes it possible to remove the inaccuracy of $g(kl)$ caused by statistical error in the numerical PDF $P(\chi_1,\chi_2,l)$. The deviations of the direct calculations from the analytical formula (36) remain approximately the same (Fig. 8). This means that the discrepancy seems to result mainly from the spread of k in the initial wave function.

V. CONCLUSION

We considered the statistical properties of time-dependent wave functions for two classically chaotic systems: the $S4$ billiard and the elbow-shaped scattering system. In order to understand statistical properties of spatially irregular wave functions, we have gone beyond the distribution functions of $\chi=\mathrm{Re}\psi$ and $\eta=\mathrm{Im}\psi$ and introduced their spatial pair distribution functions. The pair distribution functions are very sensitive to characteristic features of fluctuations.

Analysis of our numerical results shows that the spatial fluctuations of the real and imaginary parts of irregular

wave functions, at least at short distances comparable to k^{-1}, where k is the average wave vector, are Gaussian, in agreement with the predictions based on the plane-wave superposition approximation. Thus, our wave-packet calculations have confirmed the validity of the representation of an irregular wave function as a superposition of many plane waves with random phases and isotropic distribution of wave-vector directions.

ACKNOWLEDGMENTS

Funding for this research was provided by the Queen's Advisory Research Council and by the Networks of Centres of Excellence in Molecular and Interfacial Dynamics (CEMAID), supported by the Government of Canada. Partial support for D.M.W. was provided by NSERC of Canada.

[1] B. Eckhardt, Phys. Rep. **163**, 205 (1988).
[2] T. A. Brody, J. Flores, J. B. French, P. A. Mello, A. Pandey, and S. S. M. Wong, Rev. Mod. Phys. **53**, 385 (1981).
[3] P. Gaspard and S. A. Rice, J. Chem. Phys. **90**, 2242 (1989); **90**, 2255 (1989).
[4] R. Blumël and U. Smilansky, Phys. Rev. Lett. **60**, 477 (1988); Physica D **36**, 111 (1989); Phys. Rev. Lett. **64**, 241 (1990).
[5] E. Doron, U. Smilansky, and A. Frenkel, Phys. Rev. Lett. **65**, 3072 (1990); Physica D **50**, 367 (1991).
[6] B. Eckhardt, Physica D **33**, 89 (1988).
[7] U. Smilansky, in *Chaos and Quantum Physics,* edited by M. J. Giannoni, A. Voros, and J. Zinn-Justin (North-Holland, Amsterdam, 1990).
[8] R. Blumël, in *Directions in Chaos,* edited by H. Bai-Lin, D. H. Feng, and J. M. Yuan (World Scientific, Singapore, 1991), Vol. 4.
[9] H. A. Weidenmüller, Comments Nucl. Part. Phys. **16**, 199 (1986).
[10] M. Shapiro and G. Goelman, Phys. Rev. Lett. **53**, 1714 (1984).
[11] S. W. McDonald and A. N. Kaufman, Phys. Rev. A **37**, 3067 (1988).
[12] R. Aurich and F. Steiner, Physica D **48**, 445 (1991).
[13] P. Brumer and M. Shapiro, in *Evolution of Size Effects in Chemical Dynamics Part 1,* edited by I. Prigogine and S. A. Rice (Wiley, New York, 1988); M. Shapiro, J. Ronkin, and P. Brumer, Chem. Phys. Lett. **148**, 177 (1988); Ber. Bunsenges. Phys. Chem. **92**, 212 (1988).
[14] M. V. Berry, J. Phys. A **10**, 2083 (1977).
[15] N. G. Van Kampen, *Stochastic Processes in Physics and Chemistry* (North-Holland, Amsterdam, 1981).
[16] H. H. Hulburt and J. O. Hirschfelder, J. Chem. Phys. **11**, 276 (1943).
[17] A. Lo, B. L. Lan, and D. M. Wardlaw (unpublished).
[18] E. A. McCullough and R. E. Wyatt, J. Chem. Phys. **54**, 3578 (1971).
[19] H. F. Harmuth, J. Math. Phys. **36**, 269 (1957).
[20] A. Askar and A. S. Cakmak, J. Chem. Phys. **68**, 2794 (1978).
[21] K. M. Christoffel and P. Brumer, Phys. Rev. A **33**, 1309 (1986).
[22] P. M. Agrawal and L. M. Raff, J. Chem. Phys. **74**, 5076 (1981).